Dirac spinons intermingled with singlet states in the random kagome antiferromagnet $YCu_3(OD)_{6+x}Br_{3-x}$ ($x = 0.5$)

Chanhyeon Lee,[1,*] Wonjun Lee,[2,*] Suheon Lee,[2] Takayoshi Yamanaka,[3] Sungmin Jeon,[4] Joydev Khatua,[4] Hiroyuki Nojiri,[3,†] and Kwang-Yong Choi[4,‡]

[1]*Department of Physics, Chung-Ang University, Seoul 06974, Republic of Korea*

[2]*Center for Artificial Low Dimensional Electronic Systems, Institute for Basic Science, Pohang 37673, Republic of Korea*

[3]*Institute for Materials Research, Tohoku University, Sendai 980-8577, Japan*

[4]*Department of Physics, Sungkyunkwan University, Suwon 16419, Republic of Korea*

(Received 14 January 2024; revised 5 July 2024; accepted 30 July 2024; published 15 August 2024)

We elucidate the ground state nature and low-energy spin dynamics of the $s = 1/2$ near-perfect kagome antiferromagnet $YCu_3(OD)_{6+x}Br_{3-x}$ ($x = 0.5$) using ^{63}Cu nuclear quadrupole resonance (NQR) and muon spin relaxation/rotation (μSR) techniques. Our combined ^{63}Cu NQR and μSR data, along with the inverse Laplace transform analysis, reveal an inhomogeneous ground state comprising the majority of a gapless spin liquid intermingled with a minor fraction of spin singlets with varying energy gaps. Furthermore, the ^{63}Cu NQR relaxation rate evinces distinct signatures of Dirac spinons, featuring a power-law dependence of $1/T_1 \sim T^{\eta}$ with $\eta = 1.35$ at temperatures below $0.13J$ ($\cong$8 K). Our results demonstrate that a kagome lattice endowed with specific exchange randomness provides a prominent platform for exploring Dirac fermions in magnetic insulators.

DOI: 10.1103/PhysRevB.110.064418

I. INTRODUCTION

The $s = 1/2$ kagome Heisenberg antiferromagnets (KHAFs) have long been considered a holy grail in the quest for quantum spin liquids (QSLs) [1]. Recently, a growing body of numerical calculations supports the existence of either a $\mathbb{Z}_2$ gapped QSL or a gapless U(1) Dirac QSL [2–5]. However, perturbations inevitable in real materials cause transitions from the sought-after QSL to neighboring phases such as chiral spin liquids, valence bond solids (VBSs), and magnetically ordered states [6].

From a materials standpoint, the discovery of herbertsmithite $ZnCu_3(OH)_6Cl_2$ in 2005 has ignited a surge of research activity [7–10]. Subsequent investigations into its polymorph and variations, including kapellasite, Zn-brochantite, and Zn-barlowite, have uncovered intriguing QSL characteristics such as fractionalized spin excitations and the absence of long-range magnetic order [11–16]. Nonetheless, the presence of Zn-Cu antisite mixing gives rise to a coexistence of spatially varying gapped singlets and a gapless disordered state [17], posing formidable challenges in comprehending the intrinsic kagome physics.

In this context, the recently synthesized $YCu_3(OH)_{6+x}X_{3-x}$ (X = halogen) compounds stand out, primarily owing to their tunable structure, which can vary from a perfect kagome lattice to a distorted structure depending on the composition [18–22]. Unlike herbertsmithite, $YCu_3(OH)_{6+x}X_{3-x}$ lacks intersite mixing due to the substantial difference in the ionic radii of Y^{3+} and Cu^{2+}. Notably, $YCu_3(OH)_{6+x}Br_{3-x}$ ($x \sim 0.5$) (abbreviated as YCu_3-$Br_{2.5}$) defies conventional magnetic ordering down to 50 mK and displays thermodynamic and spectroscopic signatures of Dirac spinons, including a low-temperature T^2 specific heat, spinon excitations with a conical structure, and superlinear magnetic Raman excitations [23–30]. However, thermal conductivity measurements indicate the presence of a spin gap that seems to contradict gapless excitations at the Dirac nodal points [31]. Furthermore, the observed Dirac nodes deviate in their position and number within the Brillouin zone from the predictions of the mean-field KHAF model [2,32]. Exchange randomness, arising from a random occupation of Br^- and OH^-, may be responsible for such modifications, warranting further exploration.

In this paper, we combine muon spin relaxation/rotation (μSR) and ^{63}Cu nuclear quadrupole resonance (NQR) techniques to examine the purported Dirac spinons in YCu_3-$Br_{2.5}$. Our local-probe data unveil the prevalence of a Dirac-like QSL state, coexisting with a minority of spin singlets. This observation underscores the persistence of Dirac spinons against exchange randomness. Additionally, the inhomogeneous ground state reveals deeper insights into the seemingly conflicting gapped and gapless behaviors reported among different measurement techniques.

II. EXPERIMENTAL DETAILS

Single crystals of $YCu_3(OD)_{6.5}Br_{2.5}$ were synthesized by a hydrothermal method as detailed in Ref. [28].

*These authors contributed equally to this work.
†Contact author: hiroyuki.nojiri.e8@tohoku.ac.jp
‡Contact author: choisky99@skku.edu

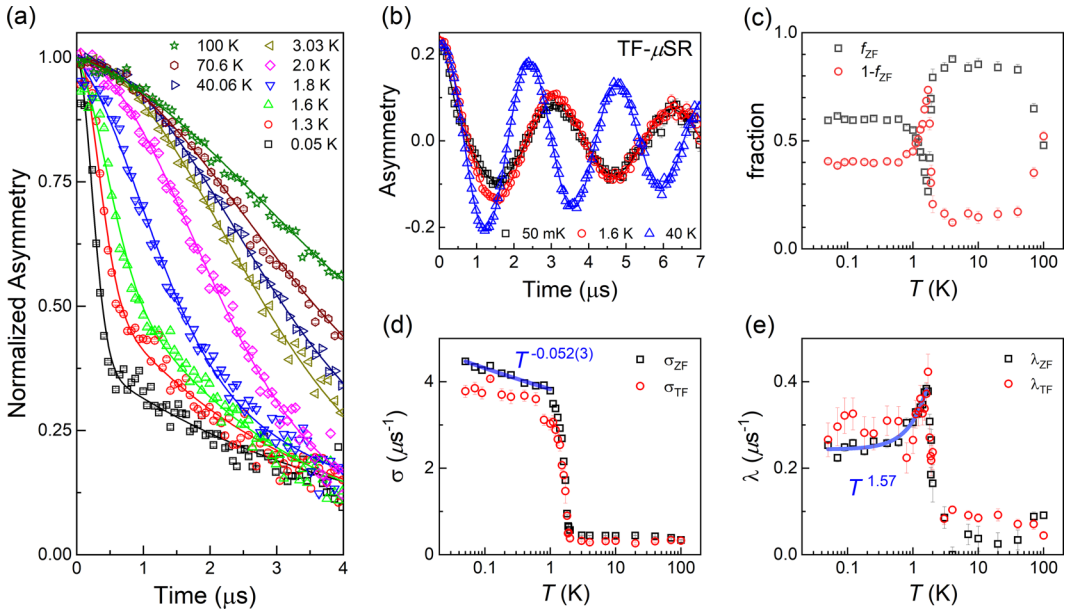

FIG. 1. (a) Temperature dependence of normalized ZF-μSR spectra. (b) TF-μSR spectra at selected temperatures. (c) Fraction of the Gaussian relaxing component. (d) Muon relaxation rates σ_{ZF} (black squares) and σ_{TF} (red circles) plotted against temperature on a semilogarithmic scale. (e) Semilog plot of λ_{ZF} (black squares) and λ_{TF} (red circles) vs temperature, extracted from the relaxation fitting function detailed in the main text. The solid lines present their power-law dependence below 1 K.

μSR experiments were conducted at the M15 and M20 beamlines in TRIUMF (Vancouver, Canada). The single crystals were loaded into a dilution refrigerator for low-T measurements ($T = 0.05$–4 K) at the M15 beamline. Higher-temperature measurements ($T = 1.8$–100 K) were performed on samples packed by Al-mylar tape using the LAMPF spectrometer at the M20 beamline. Zero-field (ZF) and transverse-field (TF) μSR data at $T = 1.8$ K were used to quantify the background fraction of signals arising from the silver sample holder in the dilution refrigerator. All obtained μSR data were fitted utilizing the MUSRFIT software package [33].

The ^{63,65}Cu ($I = 3/2$) NQR spectra were acquired using a standard Hahn-echo sequence with a $\pi/2$ pulse length of $\tau_{\pi/2} = 15$ μs. While tracking all peaks, we varied the frequency point by point with a 0.01 MHz interval. The spin-lattice relaxation rate $1/T_1$ was measured by the saturation recovery technique with multiple saturation pulses and $\tau_{\pi/2} = 2$–3 μs. The nuclear magnetization recovery curves $M(t)$ for the central transition line with elapsed time t were fitted to the expression $[M_\infty - M(t)]/M_\infty = A[e^{-(3t/T_1^{str})^\beta}]$, where A is a fitting parameter and β is the stretched exponent. The $1/T_1$ difference between ^{65}Cu and ^{63}Cu was found to be marginal, approximately 3%. In addition to the stretched fit, we further analyzed $M(t)$ using the inverse Laplace transform (ILT) method based on Tikhonov regularization [34,35]. Assuming that $1/T_1$ is spatially varied, the histogram $P(1/T_1)$, representing the probability density for the nuclear spins with each relaxation rate, was deduced using the expression $M(t)/M_\infty = \sum_j P(1/T_{1j})[1 - \exp(-3t/T_{1j})]$ with $\sum_j P(1/T_{1j}) = 1$. Here, $1/T_{1j}$ denotes the jth value of the distributed $1/T_1$. In deriving $P(1/T_1)$, we ensured the validity of our fitting procedure by following the methodology outlined in Ref. [35]. Furthermore, we stress that our fitting protocol was successfully applied to disordered Kitaev materials $H_3LiIr_2O_6$ and hyperkagome antiferromagnet $Na_{4-x}Ir_3O_8$ [36,37].

III. RESULTS

A. Muon spin relaxation/rotation

Figures 1(a) and 1(b) present the ZF- and TF-μSR spectra of YCu_3-$Br_{2.5}$. With decreasing temperature, the muon spin polarization undergoes rapid relaxation in the initial time window $t = 0$–1 μs. Nonetheless, the lack of coherent oscillation down to 50 mK and a 1/3 recovery of the muon polarization at long times precludes the occurrence of static magnetic ordering.

For a quantitative analysis, we modeled the ZF-μSR spectra as the sum of a Gaussian and a simple exponential function, along with a background signal a_{bkg}: $P_{ZF}(t) = f_{ZF}\exp(-\frac{1}{2}\sigma_{ZF}^2 t^2) + (1 - f_{ZF})\exp(-\lambda_{ZF}t) + a_{bkg}$. Here, σ_{ZF} and λ_{ZF} are the zero-field muon relaxation rates, and f_{ZF} is the fraction of the Gaussian relaxing component. Additionally, the TF-μSR spectra were fitted using the relaxation function, $a_{TF}P_{TF}(t) = a_{TF}[f_{TF}\exp(-\frac{1}{2}\sigma_{TF}^2 t^2) + (1 - f_{TF})\exp(-\lambda_{TF}t)]\cos(2\pi f_\mu t + \phi)$, where a_{TF} is the initial asymmetry from the sample, f_μ is the muon Larmor precession frequency, and ϕ is the initial phase. Noteworthy is that Gaussian-shaped relaxation has been reported in kagome systems $SrCo_8Ga_4O_{19}$ [38] and $YBaCo_4O_{7+\delta}$ [39], suggesting the presence of a local field infrequently detected within the fluctuation time of muons. In this vein, the concurring Gaussian and exponential relaxation functions allude to an inhomogeneous mixture of distinctly behaving spins.

The resulting fit parameters are summarized in Figs. 1(c)–1(e), revealing similar trends between the σ_{ZF} (λ_{ZF}) and σ_{TF} (λ_{TF}) data. As depicted in Fig. 1(c), the Gaussian and exponential relaxing components are nearly equal at 100 K. As the temperature is lowered, the fraction f_{ZF} exhibits a steep increase, reaching ≈0.84 at $T = 40$ K, followed by a sharp drop to 0.26 at $T_f = 1.6$ K. Eventually, f_{ZF} recovers to a value of ≈0.6 below 1 K. These two anomalies are associated with the low- and high-temperature peaks observed in the specific heat, corresponding to the spin freezing and spin-range spin ordering, respectively [28]. The fraction f_{TF} displays similar behavior to f_{ZF} (not shown here).

Evident from Fig. 1(d), both σ_{ZF} and σ_{TF} show a steep increment with lowering temperature through 2 K, indicating the slowdown of spin correlations. For temperatures below 1 K, $\sigma_{ZF}(T)$ exhibits a weak power-law increase of $\propto T^{-0.052}$. We note that the values of $\sigma_{ZF}(\sigma_{TF}) \sim 4$–$4.5\ \mu s^{-1}$ are an order of magnitude larger than $\lambda_{ZF}(\lambda_{TF}) \sim 0.25$–$0.3\ \mu s^{-1}$. In the fast-fluctuation regime above 2 K, the exchange fluctuation rate is given by $\nu = \sqrt{z}JS/\hbar \sim 8.25 \times 10^{12}$ s [40], where $z = 4$ is the nearest-neighbor coordination number and $J \sim 60$ K is the exchange interaction [28]. Using the relation $\lambda = \Delta^2/\nu$ in the motional narrowing limit, $\lambda_{ZF}(T = 100\ K) = 0.0912\ \mu s^{-1}$ yields a distribution width of local magnetic fields $\Delta/\gamma_\mu = 7.20(1)$ kG.

On the contrary, a discernible peak at T_f observed in λ_{ZF} and λ_{TF} [see Fig. 1(e)] indicates the partial freezing of local magnetic moments at approximately 1.6 K. On cooling below $T < T_f$, $\lambda_{ZF}(T)$ follows a $T^{1.57}$ power-law decrease with a residual relaxation rate $\lambda_{ZF}(T = 50\ mK) = 0.25\ \mu s^{-1}$. Similar behavior has been observed in a range of geometrically frustrated magnets, including $Dy_2Ti_2O_7$ [41], $Y_2Mo_2O_7$ with $\lambda \propto T^{2.1}$ for $T < 22$ K [42], and $RbAg_2Cr[VO_4]_2$ with $\lambda \propto T^{0.9}$ below 20 K [43]. The substantial residual spin dynamics below $T < T_f$ signifies the persistence of low-energy magnetic fluctuations within the μSR time window.

Next, we move on to the muon decoupling experiments to further characterize spin-spin correlations. Figures 2(a) and 2(b) present the longitudinal field (LF)-μSR spectra measured at $T = 50$ mK and 10 K. It is evident that our highest applied LF of 4000 G is insufficient to attain full suppression of muon spin depolarization, which evinces the predominance of dynamically fluctuating spins. The same relaxation function utilized to fit the ZF-μSR data is also used to model the LF-μSR data for temperatures below T_f.

As shown in Fig. 2(c), the LF dependence of $\sigma_{LF}(B)$ at $T = 50$ mK initially decreases rapidly, and then levels out above 2000 G. We find that $\sigma_{LF}(B, T = 50\ mK)$ is well described by the Redfield equation $\sigma_{LF}(B) = 2\gamma_\mu^2\langle B_{loc}^2\rangle\nu/(\nu^2 + \gamma_\mu^2 B_{LF}^2)$. Here, γ_μ is the muon gyromagnetic ratio and $\langle B_{loc}\rangle$ is the time average of the fluctuating internal field at muon sites. The estimated values of $\nu = 36.89(1)\ \mu s^{-1}$ and $\langle B_{loc}\rangle = 105.44(7)$ G are roughly five times slower and larger than those of herbertsmithite, which are $\nu = 150$ MHz and $\langle B_{loc}\rangle = 18$ G, respectively [7]. Meanwhile, $\lambda_{LF}(B)$ [open blue squares in Fig. 2(d)] exhibits a two-stage decrease with increasing LF, suggesting the development of complex spin correlations.

For the $T = 10$ K LF-μSR spectra, we model them as the relaxation function, $a_0 P_{LF}(t) = a_0[fG_{LF}(t) + (1 - f)\exp(-\lambda_{LF}t)] + a_{bkg}$, where a_0 is the initial asymmetry for a LF configuration. Here, $G_{LF}(t)$ describes a system having static magnetic moments under LF conditions [44], given by

$$G_{LF}(t) = 1 - \frac{2\sigma^2}{(2\pi\nu)^2}\left[1 - \exp\left(-\frac{1}{2}\sigma^2 t^2\right)\cos(2\pi\nu t)\right] + \frac{2\sigma^4}{(2\pi\nu)^3}\int_0^\tau \exp\left(-\frac{1}{2}\sigma^2\tau^2\right)\sigma(2\pi\nu\tau)d\tau.$$

By analyzing $\lambda_{LF}(B, T = 10\ K)$ based on the Redfield formula, we obtain $\nu = 0.26(9)$ MHz and $\langle B_{loc}\rangle = 1.85(6)$ G.

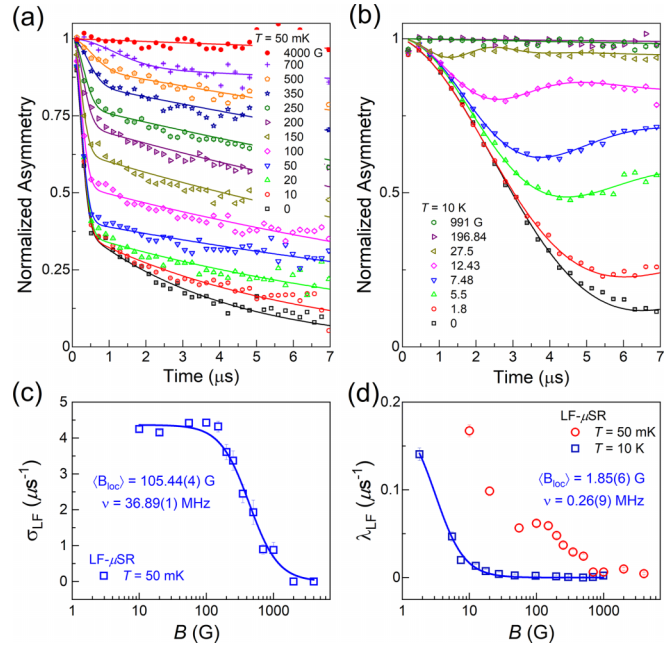

FIG. 2. Longitudinal field dependence of normalized LF-μSR spectra at (a) $T = 50$ mK and (b) $T = 10$ K. The muon relaxation rate σ_{LF} (c) at $T = 50$ mK and λ_{LF} (d) at $T = 50$ mK (open blue squares) $T = 10$ K (pink circles) as a function of applied longitudinal fields. The solid lines are the fit using the Redfield formula.

B. Nuclear quadrupole resonance

We turn to the zero-field ^{63,65}Cu NQR spectra. As exhibited in Fig. 3(a), two distinct lines are seen at $^{65}\nu_Q = 7.2(1)$ MHz and $^{63}\nu_Q = 7.7(5)$ MHz whose frequency ratio matches that of nuclear quadrupole moments (Q): $^{63}\nu_Q/^{65}\nu_Q = {}^{63}Q/{}^{65}Q \approx 1.08$ [45]. With decreasing temperature, the ^{63,65}Cu NQR line shapes experience a power-law $T^{-0.33}$ broadening above 1 K and $T^{-0.80}$ below 1 K [see pink circles in Fig. 3(b)], suggesting enhanced magnetic correlations through T_f. Nonetheless, no apparent NQR shift is observable in their spectral lines, possibly due to the broader linewidth of the ^{63,65}Cu NQR compared to the thermal shift of $^{63,65}\nu_Q$.

We next discuss the ^{63}Cu nuclear spin-lattice relaxation rate $1/T_1$, which pertains to low-energy spin excitations integrated over $\mathbf{q}$ at the NQR frequency ω_0. In determining $1/T_1$, we attempted to analyze $M(t)$ using two alternative methods: a conventional stretched exponential fit versus an ILT fit. Figure 3(c) compares the representative fits at $T = 0.5$ K, showing that the ILT fit (solid line) provides a somewhat better description of $M(t)$ than the stretched fit (dotted line).

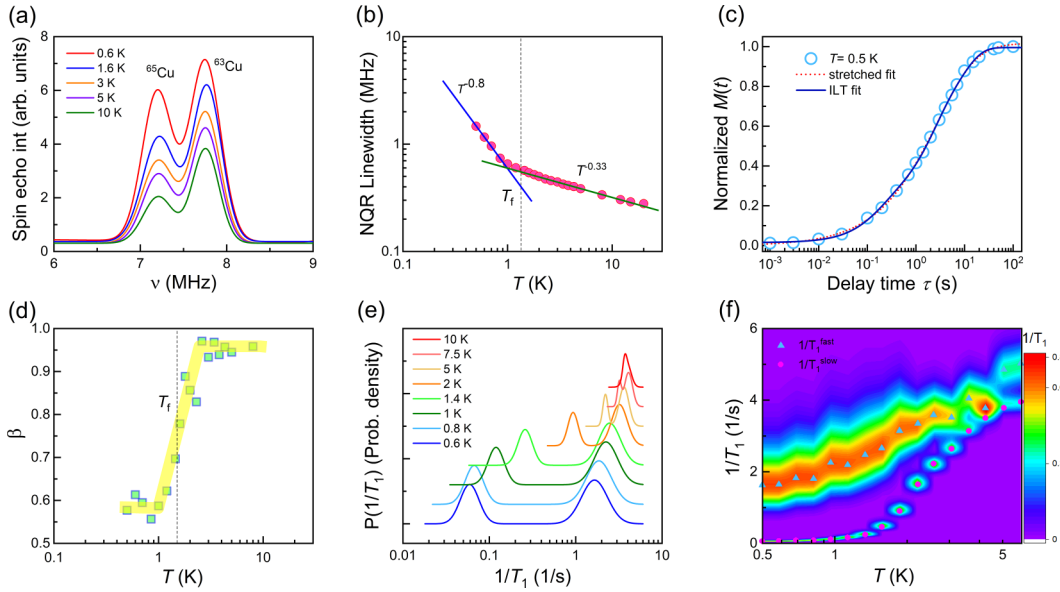

FIG. 3. (a) ^{63,65}Cu NQR spectra of $YCu_3(OD)_{6.5}Br_{2.5}$ at selected temperatures. (b) Temperature dependence of the NQR linewidth on a semilogarithmic scale. The vertical dashed line indicates the spin-freezing temperature T_f. The solid lines depict power-law behaviors. (c) Stretched (dotted line) and ILT (solid line) fits of normalized $M(t)$ at $T = 0.5$ K. (d) Semilog plot of the stretched exponent β vs temperature. The shaded thick line is a guide to the eye. (e) Distribution function $P(1/T_1)$ plotted against temperature in a semilog scale. (f) Color contour plot of $P(1/T_1)$ in the temperature-$1/T_1$ plane. The triangles and circles represent the center positions of the two separate distributions.

As plotted in Fig. 3(d), on cooling through T_f, the stretched exponent β undergoes a strong reduction from ≈0.96 to 0.57, implying the development of a significant distribution of $1/T_1$ due to spin freezing.

In Fig. 3(e), we show a semilog plot of the probability density function $P(1/T_1)$ vs $1/T_1$, extracted from the ILT analysis of $M(t)$. The corresponding color contour plot of $P(1/T_1)$ vs T is further displayed in Fig. 3(f). Here, $1/T_1$ on the y axis is presented in a linear scale, in contrast to the logarithmic scale used on the x axis in Fig. 3(e). Notably, a two-peak structure evolves progressively from an initially single line at $\sim 4\ s^{-1}$ below $T = 10$ K. By deconvoluting the $P(1/T_1)$ histogram into two Gaussian profiles, we trace separately the thermal location of the peaks: the slower T_1^{slow} (pink circles) and faster T_1^{fast} (green triangles) components. Remarkably, T_1^{slow} is almost two orders of magnitude smaller than T_1^{fast}.

To shed light on the underlying nature of spin dynamics, the center positions of the slower and slower relaxation components are plotted as a function of temperature in Fig. 4(a). $T_1^{fast}(T)$ (green triangles) exhibits a $T^{1.35}$ power-law decrease as $T \to 0$ K from 8 K, which is characteristic of a gapless QSL ground state. Conversely, the notable suppression of $T_1^{slow}(T)$ (pink circles) below 8 K suggests the emergence of gapped excitations. The absence of activation behavior means varying spin gaps rather than a well-defined gap energy (not shown here). Further, the lacking constant gap is not compatible with a chiral spin-liquid scenario [6]. To validate the extracted $P(1/T_1)$ through the ILT procedure, we compare T_1^{str} (blue stars) with the center of gravity of $P(1/T_1)$ [crosses in Fig. 4(a)]. The near-perfect overlap between these values lends strong support to the existence of two-component spin dynamics, which cannot be adequately captured by the stretched exponential analysis.

The temperature dependence of $1/T_2$ is shown in the left y axis of Fig. 4(b). $1/T_2$ (pink circles) exhibits a weak power-law reduction with $1/T_2 \sim T^{0.15}$ in the $T = 1$–5 K range and undergoes a steeper decrease below 1 K. Notably, $1/T_2$ mirrors the thermal evolution of the NQR linewidth [see Fig. 3(b)], although the power-law temperature window is reduced down to 5 K. The right y axis of Fig. 4(b) presents the singlet fraction (f_S) of Cu^{2+} sites obtained by the integration of the $P(1/T_1)$ curve [data shown in Fig. 3(e)]. On cooling, $f_S(T)$ shows a steady decrease from the initial value of $f_S = 0.31$ down to 2 K, and then undergoes a rapid drop through T_f, and eventually flattens out with $f_S \approx 0.02$ below 1 K.

Before proceeding, we discuss the differences in the temperature dependencies of the muon relaxation rate (λ) and the ^{63,65}Cu $1/T_1$. In sharp contrast to λ [see Fig. 1(e)], $1/T_1$ shows no signatures of spin freezing at T_f. One possible explanation is that the temporal structure of spin fluctuations hinges on the time domain probed by NMR and μSR in the presence of magnetic inhomogeneities. Another possibility involves the modified form factor of the implanted muons. In magnetic oxides, the positive muon typically resides near the negatively charged oxygen ions. In YCu_3-$Br_{2.5}$, the Br2/O2 sites are randomly occupied, unlike the O1 site, leading to variations in the form factor. Therefore, the on-site ^{63,65}Cu nuclei serve as a better probe of intrinsic spin dynamics. Altogether, our ILT analysis of ^{63}Cu NQR reveals that the ground state of YCu_3-$Br_{2.5}$ is predominantly characterized by a gapless quantum disordered state, intermingled with a few percentages of random singlets. A mixture of these two

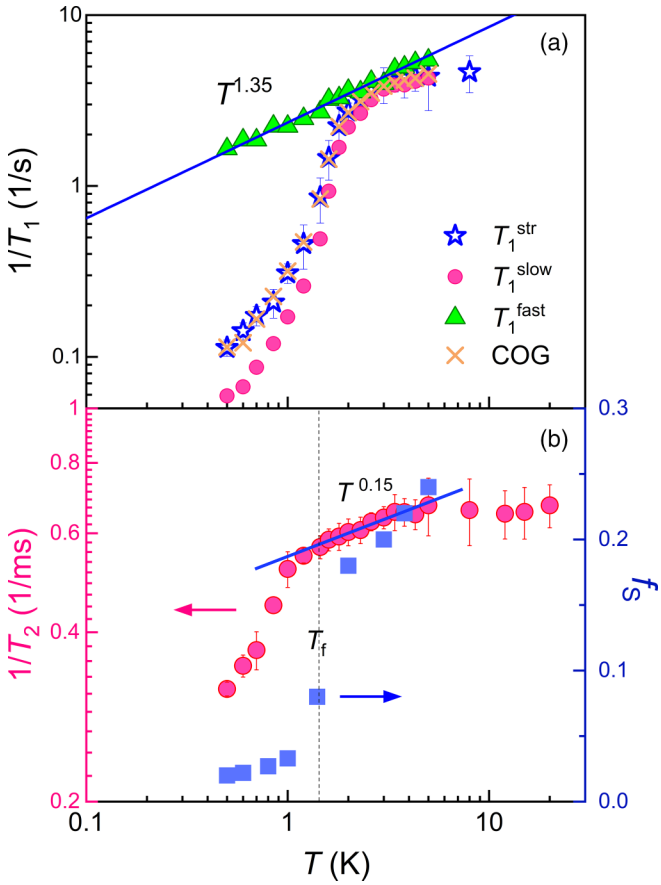

FIG. 4. (a) Temperature dependence of $1/T_1^{slow}$ (pink circles), $1/T_1^{fast}$ (green triangles), $1/T_1^{str}$ (blue stars), and the center of gravity (COG; crosses). (b) Temperature dependence of the spin-spin relaxation rate $1/T_2$ (left y axis) and the singlet fraction f_S of Cu sites (right y axis) plotted on a log-log scale. The solid lines represent the power-law dependence of the ^{63,65}Cu nuclear relaxation rates. The vertical dashed line marks the spin-freezing temperature T_f.

distinct states appears to occur inevitably in the presence of exchange randomness [46,47].

IV. DISCUSSION AND CONCLUSION

With the help of μSR and ^{63}Cu NQR techniques, we decipher the inhomogeneous nature of the alleged QSL ground state in YCu_3-$Br_{2.5}$, which holds remarkable similarities with Zn-barlowite and herbertsmithite [17]. In both YCu_3-$Br_{2.5}$ and herbertsmithite, we identify the characteristic temperature $T^* = 0.13$–$0.16J$, below which heterogeneous magnetic correlations emerge. Despite these apparent resemblances, there exists a fundamental disparity between YCu_3-$Br_{2.5}$ and herbertsmithite. In YCu_3-$Br_{2.5}$, unlike herbertsmithite, the gapless component obeys a power-law behavior of $1/T_1 \sim T^{\eta}$, which is reminiscent of Dirac fermions predicted in gapless QSL [2,3]. Furthermore, the singlet fraction diminishes with small residual fraction as $T \to 0$ K, opposite to the steady growth of the singlet fraction of Cu sites observed for Zn-barlowite and herbertsmithite [17].

This contrasting behavior relies on the distinct species of quenched disorders. In Zn-barlowite and herbertsmithite, antisite cation mixing and dangling bonds on kagome lattices generate abundant low-lying excitations, which may cover a small spectral weight emanating from the Dirac nodal points. In this situation, random-singlet-type states become dominant over the hypothesized Dirac spin liquid. As to YCu_3-$Br_{2.5}$, the exchange randomness of three different Js as a leading perturbation enlarges the Brillouin zone and brings about gapped excitations of an order of ~10 K [25,28]. In this case, the alleged Dirac spinons lying below 10 K may be hardly affected by the sizable bond randomness.

We further discuss the observed ^{63}Cu NQR results in light of mean-field calculations for the isotropic KHAF model [3]. According to the mean-field KHAF model, the Dirac spinon is well defined in the energy range below the spinon bandwidth $W \approx 0.25J$ ($\cong$15 K). Notably, a recent INS study confirmed the Dirac-like linear dispersion up to 7 K [27]. Consistently with the INS results, the onset temperature ($\sim 0.13J \approx 8$ K) of the power-law $1/T_1$ amounts to half of the energy scale of W. Admittedly, the $1/T_1 \sim T^{1.35}$ behavior alone is insufficient to confirm the presence of Dirac spinons. Nonetheless, the Dirac conical excitations observed through INS [27] suggest that the near-linear $1/T_1$ dependence may originate from Dirac spinons. Unlike $\lambda(T)$ in Fig. 1(e) and $1/T_2$ in Fig. 4(b), the power-law dependence of $1/T_1$ is barely affected by the weak spin freezing at T_f. This implies the robustness of Dirac spinon excitations against the small perturbation of $T_f/W \sim 0.1$, albeit not in an entirely pristine form.

Secondly, our ^{63}Cu NQR data yield the exponent $\eta_{\rm exp} = 1.35$ [see Fig. 4(a)], associated with the scaling dimension through the relation $\eta_{N(m)} = 2\Delta_{N(m)} - 1$ [3]. Here, $\Delta_N \approx 1.73$ represents the correlations of VBS order, while $\Delta_m \approx 1.06$ is $\mathbf{q} = \mathbf{0}$ magnetic correlations. The experimental value of $\Delta_{\rm exp} \approx 1.18$ means that YCu_3-$Br_{2.5}$ is on the verge of the $\mathbf{q} = \mathbf{0}$ magnetic instability. Actually, our μSR data detect the weak freezing of magnetic moments in this material [see Fig. 1(e)].

The prevailing Dirac spinons detected by ^{63}Cu NQR, coexisting with a small fraction of singlet states, align well with various experimental observations such as the T^2 specific heat, Dirac conical excitations by INS, and superlinear ω dependence of Raman spinon scattering [23–28,30]. On the other hand, the semimetallic nature of putative Dirac spinon excitations and the presence of random singlets account for the lack of itinerant quasiparticles suggested by thermal conductivity measurements [31], as the density of states of the low-energy quasiparticles is insufficient to carry heat. All in all, our μSR and NQR results reveal an inhomogeneous ground state that behaves more intriguingly than a simple spin gap or gapless QSL.

To conclude, we have thoroughly investigated the intricate ground state and its low-energy spin dynamics of an $s = 1/2$ Cu-based kagome compound YCu_3-$Br_{2.5}$ subject to exchange randomness. Our magnetic resonance measurements uncover that a heterogeneous ground state is overwhelmingly dominated by the much sought-after Dirac spinons. The near realization of these elusive Dirac spinons in random kagome lattices raises the question of their relevance to a Dirac QSL predicted in the disorder-free, isotropic KAHF model.

ACKNOWLEDGMENTS

The work at SKKU was supported by the National Research Foundation (NRF) of Korea (Grants No. 2020R1A2C3012367 and No. 2020R1A5A1016518). S.L. acknowledges support from the Institute for Basic Science (IBS-R014-Y2). A portion of the research was performed in the GIMRT program at IMR, Tohoku University. We thank B. S. Hitti for assistance with the SR measurements.

[1] S. Yan, D. A. Huse, and S. R. White, Spin-liquid ground state of the $S = 1/2$ kagome Heisenberg antiferromagnet, Science **332**, 1173 (2011).

[2] Y. Ran, M. Hermele, P. A. Lee, and X.-G. Wen, Projected-wave-function study of the spin-1/2 Heisenberg model on the kagomé lattice, Phys. Rev. Lett. **98**, 117205 (2007).

[3] M. Hermele, Y. Ran, P. A. Lee, and X.-G. Wen, Properties of an algebraic spin liquid on the kagome lattice, Phys. Rev. B **77**, 224413 (2008).

[4] S. Depenbrock, I. P. McCulloch, and U. Schollwöck, Nature of the spin-liquid ground state of the $S = 1/2$ Heisenberg model on the kagome lattic, Phys. Rev. Lett. **109**, 067201 (2012).

[5] B. Bernu and C. Lhuillier, Spin susceptibility of quantum magnets from high to low temperatures, Phys. Rev. Lett. **114**, 057201 (2015).

[6] L. Messio, S. Bieri, C. Lhuillier, and B. Bernu, Chiral spin liquid on a kagome antiferromagnet induced by the Dzyaloshinskii-Moriya interaction, Phys. Rev. Lett. **118**, 267201 (2017).

[7] P. Mendels, F. Bert, M. A. de Vries, A. Olariu, A. Harrison, F. Duc, J. C. Trombe, J. S. Lord, A. Amato, and C. Baines, Quantum magnetism in the paratacamite family: Towards an ideal kagomé lattice, Phys. Rev. Lett. **98**, 077204 (2007).

[8] P. Mendels and F. Bert, Quantum kagome antiferromagnet $ZnCu_3(OH)_6Cl_2$, J. Phys. Soc. Jpn. **79**, 011001 (2010).

[9] M. R. Norman, *Colloquium*: Herbertsmithite and the search for the quantum spin liquid, Rev. Mod. Phys. **88**, 041002 (2016).

[10] M. P. Shores, E. A. Nytko, B. M. Barlett, and D. G. Nocera, A structurally perfect $S = 1/2$ kagomé antiferromagnet, J. Am. Chem. Soc. **127**, 13462 (2005).

[11] T.-H. Han, J. S. Helton, S. Chu, D. G. Nocera, J. A. Rodriguez-Rivera, C. Broholm, and Y. S. Lee, Fractionalized excitations in the spin-liquid state of a kagome-lattice antiferromagnet, Nature (London) **492**, 406 (2012).

[12] B. Fåk, E. Kermarrec, L. Messio, B. Bernu, C. Lhuillier, F. Bert, P. Mendels, B. Koteswararao, F. Bouquet, J. Ollivier, A. D. Hillier, A. Amato, R. H. Colman, and A. S. Wills, Kapellasite: A kagome quantum spin liquid with competing interactions, Phys. Rev. Lett. **109**, 037208 (2012).

[13] K. Tustain *et al.*, From magnetic order to quantum disorder in the Zn-barlowite series of $S = 1/2$ kagome antiferromagnets, npj Quantum Mater. **5**, 74 (2020).

[14] Z. Feng *et al.*, Gapped spin-1/2 spinon excitations in a new kagome quantum spin liquid compound $Cu_3Zn(OH)_6FBr$, Chin. Phys. Lett. **34**, 077502 (2017).

[15] R. W. Smaha *et al.*, Materializing rival ground states in the barlowite family of kagome magnets: Quantum spin liquids, spin ordered and valence bond crystal states, npj Quantum Mater. **5**, 23 (2020).

[16] Y. Fu, M.-L. Lin, L. Wang *et al.*, Dynamic fingerprint of fractionalized excitations in single-crystalline $Cu_3Zn(OH)_6FBr$, Nat. Commun. **12**, 3048 (2021).

[17] J. Wang *et al.*, Emergence of spin singlets with inhomogeneous gaps in the kagome lattice Heisenberg antiferromagnets Zn-barlowite and herbertsmithite, Nat. Phys. **17**, 1109 (2021).

[18] W. Sun, Y.-X. Huang, S. Nokhrin, Y. Pan, and J.-X. Mi, Perfect kagomé lattices in $YCu_3(OH)_6Cl_3$: A new candidate for the quantum spin liquid state, J. Mater. Chem. C **4**, 8772 (2016).

[19] Q. Barthélemy, P. Puphal, K. M. Zoch, C. Krellner, H. Luetkens, C. Baines, D. Sheptyakov, E. Kermarrec, P. Mendels, and F. Bert, Local study of the insulating quantum kagome antiferromagnets $YCu_3(OH)_6O_xCl_{3-x}$ ($x = 0, 1/3$), Phys. Rev. Mater. **3**, 074401 (2019).

[20] A. Zorko, M. Pregelj, M. Gomilsek, M. Klanjsek, O. Zaharko, W. Sun, and J.-X. Mi, Negative-vector-chirality 120° spin structure in the defect- and distortion-free quantum kagome antiferromagnet $YCu_3(OH)_6Cl_3$, Phys. Rev. B **100**, 144420 (2019).

[21] P. Puphal, M. Bolte, D. Sheptyakov, A. Pustogow, K. Kliemt, M. Dressel, M. Baenitz, and C. Krellner, Strong magnetic frustration in $Y_3Cu_9(OH)_{19}Cl_8$: A distorted kagome antiferromagnet, J. Mater. Chem. C **5**, 2629 (2017).

[22] D. Chatterjee, P. Puphal, Q. Barthélemy, J. Willwater, S. Süllow, C. Baines, S. Petit, E. Ressouche, J. Ollivier, K. M. Zoch, C. Krellner, M. Parzer, A. Riss, F. Garmroudi, A. Pustogow, P. Mendels, E. Kermarrec, and F. Bert, From spin liquid to magnetic ordering in the anisotropic kagome Y-kapellasite $Y_3Cu_9(OH)_{19}Cl_8$: A single-crystal study, Phys. Rev. B **107**, 125156 (2023).

[23] X.-H. Chen, Y.-X. Huang, Y. Pan, and J.-X. Mi, Quantum spin liquid candidate $YCu_3(OH)_6Br_2[Br_x(OH)_{1-x}]$ ($x \approx 0.51$): With an almost perfect kagome layer, J. Magn. Magn. Mater. **512**, 167066 (2020).

[24] Z. Zeng, X. Ma, S. Wu, H.-F. Li, Z. Tao, X. Lu, X.-H. Chen, J.-X. Mi, S.-J. Song, G.-H. Cao, G. Che, K. Li, G. Li, H. Luo, Z. Y. Meng, and S. Li, Possible Dirac quantum spin liquid in the kagome quantum antiferromagnet $YCu_3(OH)_6Br_2[Br_x(OH)_{1-x}]$, Phys. Rev. B **105**, L121109 (2022).

[25] J. Liu, L. Yuan, X. Li, B. Li, K. Zhao, H. Liao, and Y. Li, Gapless spin liquid behavior in a kagome Heisenberg antiferromagnet with randomly distributed hexagons of alternate bonds, Phys. Rev. B **105**, 024418 (2022).

[26] F. Lu, L. Yuan, J. Zhang, B. Li, Y. Luo, and Y. Li, The observation of quantum fluctuations in a kagome Heisenberg antiferromagnet, Commun. Phys. **5**, 272 (2022).

[27] Z. Zeng, C. Zhou, H. Zhou, L. Han, R. Chi, K. Li, M. Kofu, K. Nakajima, Y. Wei, W. Zhang, D. G. Mazzone, Z. Y. Meng, and S. Li, Spectral evidence for Dirac spinons in a kagome lattice antiferromagnet, Nat. Phys. **20**, 1097 (2024).

[28] S. Jeon, D. Wulferding, Y. Choi, S. Lee, K. Nam, K. H. Kim, M. Lee, T.-H. Jang, J.-H. Park, S. Lee, S. Choi, C. Lee, H. Nojiri, and K.-Y. Choi, One-ninth magnetization plateau stabilized by

spin entanglement in a kagome antiferromagnet, Nat. Phys. **20**, 435 (2024).

[29] S. Suetsugu, T. Asaba, Y. Kasahara, Y. Kohsaka, K. Totsuka, B. Li, Y. Zhao, Y. Li, M. Tokunaga, and Y. Matsuda, Emergent spin-gapped magnetization plateaus in a spin-1/2 perfect kagome antiferromagnet, Phys. Rev. Lett. **132**, 226701 (2024).

[30] G. Zheng, Y. Zhu, K.-W. Chen, B. Kang, D. Zhang, K. Jenkins, A. Chan, Z. Zeng, A. Xu, O. A. Valenzuela, J. Blawat, J. Singleton, P. A. Lee, S. Li, and L. Li, Unconventional magnetic oscillations in kagome Mott insulators, arXiv:2310.07989.

[31] X. Hong, M. Behnami, L. Yuan, B. Li, W. Brenig, B. Büchner, Y. Li, and C. Hess, Heat transport of the kagome heisenberg quantum spin liquid candidate $YCu_3(OH)_{6.5}Br_{2.5}$: Localized magnetic excitations and a putative spin gap, Phys. Rev. B **106**, L220406 (2022).

[32] W. Zhu, S. Gong, and D. N. Sheng, Identifying spinon excitations from dynamic structure factor of spin-1/2 Heisenberg antiferromagnet on the Kagome lattice, Proc. Natl. Acad. Sci. USA **116**, 5437 (2019).

[33] A. Suter and B. M. Wojek, MUSRFIT: A free platform-independent framework for μSR data analysis, Phys. Procedia **30**, 69 (2012).

[34] Y. Q. Song *et al.*, $T_1 - T_2$ correlation spectra obtained using a fast two-dimensional Laplace inversion, J. Magn. Reson. **154**, 261 (2002).

[35] P. M. Singer, A. Arsenault, T. Imai, and M. Fujita, ^{139}La NMR investigation of the interplay between lattice, charge, and spin dynamics in the charge-ordered high-T_c cuprate $La_{1.875}Ba_{0.125}CuO_4$, Phys. Rev. B **101**, 174508 (2020).

[36] C. Lee, S. Lee, Y. Choi, C. Wang, H. Luetkens, T. Shiroka, Z. H. Jang, Y.-G. Yoon, and K.-Y. Choi, Coexistence of random singlets and disordered Kitaev spin liquid in $H_3LiIr_2O_6$, Phys. Rev. B **107**, 014424 (2023).

[37] Y. S. Choi, C. H. Lee, T. Kihara, H. Zheng, H. Nojiri, J. F. Mitchell, and K.-Y. Choi, Effects of Na deficiency on spin dynamics in the Mott insulating $Na_{4-x}Ir_3O_8$, Phys. Rev. B **109**, 144405 (2024).

[38] Y. J. Uemura *et al.*, Spin fluctuations in frustrated kagomé lattice system $SrCr_8Ga_4O_{19}$ studied by muon spin relaxation, Phys. Rev. Lett. **73**, 3306 (1994).

[39] S. Lee, W. Lee, K. J. Lee, B. Kim, B. J. Suh, H. Zheng, J. F. Mitchell, and K.-Y. Choi, Muon spin relaxation study of spin dynamics in the extended kagome systems $YBaCo_4O_{7+\delta}$ ($\delta = 0, 0.1$), Phys. Rev. B **97**, 104409 (2018).

[40] A. L. Yaouanc and P. D. de Réotier, *Muon Spin Rotation, Relaxation, and Resonance: Applications to Condensed Matter* (Oxford University Press, Oxford, UK, 2011).

[41] S. R. Dunsiger *et al.*, Spin ice: Magnetic excitations without monopole signatures using muon spin rotation, Phys. Rev. Lett. **107**, 207207 (2011).

[42] S. R. Dunsiger, R. F. Kiefl, K. H. Chow, B. D. Gaulin, M. J. P. Gingras, J. E. Greedan, A. Keren, K. Kojima, G. M. Luke, W. A. MacFarlane *et al.*, Muon spin relaxation investigation of the spin dynamics of geometrically frustrated antiferromagnets $Y_2Mo_2O_7$ and $Tb_2Mo_2O_7$, Phys. Rev. B **54**, 9019 (1996).

[43] S. Lee, R. Klauer, J. Menten, W. Lee, S. Yoon, H. Luetkens, P. Lemmens, A. Möller, and K.-Y. Choi, Unconventional spin excitations in the $S = \frac{3}{2}$ triangular antiferromagnet $RbAg_2Cr[VO_4]_2$, Phys. Rev. B **101**, 224420 (2020).

[44] R. S. Hayano, Y. J. Uemura, J. Imazato, N. Nishida, T. Yamazaki, and R. Kubo, Zero-and low-field spin relaxation studied by positive muons, Phys. Rev. B **20**, 850 (1979).

[45] Bruker Corporation, *Almanac 2011* (Bruker, Billerica, MA, 2011).

[46] L. Liu, H. Shao, Y.-C. Lin, W. Guo, and A. W. Sandvik, Random-singlet phase in disordered two-dimensional quantum magnets, Phys. Rev. X **8**, 041040 (2018).

[47] H. Kawamura and K. Uematsu, Nature of the randomness-induced quantum spin liquids in two dimensions, J. Phys.: Condens. Matter **31**, 504003 (2019).